NASA Technical Memorandum 102457

Analysis of Thermal Energy Storage Material with Change-of-Phase Volumetric Effects

Thomas W. Kerslake
Lewis Research Center
Cleveland, Ohio

and

Mounir B. Ibrahim
Cleveland State University
Cleveland, Ohio

February 1990

(NASA-TM-102457) ANALYSIS OF THERMAL ENERGY STORAGE MATERIAL WITH CHANGE-OF-PHASE VOLUMETRIC EFFECTS (NASA) 34 p CSCL 20D
N90-21974
Unclas
G3/34 0277358

NASA

ANALYSIS OF THERMAL ENERGY STORAGE MATERIAL WITH CHANGE-OF-PHASE VOLUMETRIC EFFECTS

Thomas W. Kerslake
National Aeronautics and Space Administration
Lewis Research Center
Cleveland, Ohio 44135

and

Mounir B. Ibrahim
Department of Mechanical Engineering
Cleveland State University
Cleveland, Ohio 44115

E-5244

ABSTRACT

NASA's Space Station Freedom proposed hybrid power system includes photovoltaic arrays with nickel hydrogen batteries for energy storage and solar dynamic collectors driving Brayton heat engines with change-of-phase Thermal Energy Storage (TES) devices. A TES device is comprised of multiple metallic, annular canisters which contain a eutectic composition LiF-CaF_2 Phase Change Material (PCM) that melts at 1040 K.

A moderately sophisticated LiF-CaF_2 PCM computer model is being developed in three stages considering one-, two-, and three-dimensional canister geometries, respectively. One-dimensional model results indicate that the void has a marked effect on the phase change process due to PCM displacement and dynamic void heat transfer resistance. Equally influential are the effects of different boundary conditions and liquid PCM natural convection. For the second stage, successful numerical techniques used in the one-dimensional phase change model are extended to a two-dimensional (r,z) PCM containment canister model. A prototypical PCM containment canister is analyzed and the results are discussed. Extension of numerical techniques to a three-dimensional geometry will be reported in the future.

NOMENCLATURE

c = Specific Heat, J/g-K
C5 = Constant
div = Divergence Operator
e = Specific Enthalpy, J/g
g = Gravitational Acceleration, cm/sec^2
h = Film coefficient, W/cm^2-K
H = PCM Heat of Fusion, J/g
He-Xe = Helium-Xenon Gas Mixture
i = Grid Element Index
iv = Grid Element Which Contains X_v
iv′ = Combined Grid Element
k = Thermal Conductivity, W/cm-K
L = Annular Canister Length, cm
L′ = Slab Canister Thickness, cm
LH = Liquid PCM Vertical Layer Height, cm

$LiF-CaF_2$ = Lithium Fluoride-Calcium Difluoride
MF = Mass Fraction PCM in Element iv
n3 = Constant
Nu = Nusselt Number
PCM = Phase Change Material
Pr = Prandtl Number
q = Heat flux, W/cm^2
r = Radial Coordinate, cm
R = Thermal Resistance, cm^2-K/W
Ra = Rayleigh Number
Re = Reynolds number
St = Stefan Number
t = Time, Sec
T = Temperature, K
TES = Thermal Energy Storage
u = Velocity of Void-PCM Interface, cm/sec
w = Liquid PCM Width, cm
x = One-Dimensional Coordinate, cm
X = Melt or Void Front Position, cm
XF = Mushy Zone Liquid PCM Mass Fraction
YF = Mushy Zone Liquid PCM Volume Fraction
z = Axial Coordinate, cm
• = Dot Product
∇ = Gradient Operator

<u>Greek Symbols</u>

α = Thermal Diffusivity, cm^2/sec
β = Volumetric Thermal Expansion Coefficient, 1/K
δ = Canister Wall Thickness, cm
Δr = Radial Grid Spacing, cm
Δt = Time Step, sec
ΔT = Temperature Difference, K
Δx = One-Dimensional Grid Spacing, cm
Δz = Axial Grid Spacing, cm
ϵ = Emittance
ρ = Density, g/cm^3
σ = Stefan-Boltzmann Constant, $5.67051 \times 10^{-12} W/cm^2-K^4$
υ = Kinematic Viscosity, cm^2/sec
Ψ = Dimensionless Function of Δr and r

<u>Subscripts</u>

E = Enhanced
EFF = Effective
f = He-Xe Fluid
i = Inner Radius or Grid Element Index
L = Liquid PCM
m = PCM Melt
o = Outer Radius
PCM = Phase Change Material
S = Solid PCM
v = Void
VAP = Vapor
w = Canister Wall
WS = Side Wall

1 INTRODUCTION

Electrical power for NASA's proposed Space Station Freedom will be generated by photovoltaic solar arrays initially and later augmented with Solar Dynamic Power Modules (SDPM's). The SDPM, shown conceptually in Figure 1, employs a concentrator to collect and focus solar energy on to the walls of a cylindrical cavity heat receiver where it is converted to thermal energy. A fraction of the thermal energy is transferred to a circulating working fluid to operate a heat engine and produce electrical power. The remaining thermal energy melts a eutectic composition $LiF-CaF_2$ Phase Change Material (PCM) contained in multiple canisters located concentrically around working fluid tubes running the length of the heat receiver cavity shown conceptually in Figure 2. A single PCM containment canister is shown in Figure 3. The PCM stores and releases thermal energy by undergoing phase change at its critical temperature of 1040 K. This permits continuous operation of the heat engine during the substantial eclipse periods (up to 36 minutes) of Freedom's low earth orbit. The service life requirement for the heat receiver is 30 years.

Several computer models of varying sophistication have been developed (or are currently under development) to analyze this type PCM Thermal Energy Storage (TES) canister. For example, the canister model described in [1] is very sophisticated as it predicts three-dimensional, time dependent PCM temperature, phase, and velocity (in the melt region) distributions accounting for phenomena such as buoyancy and surface-tension driven flows, dynamic void shape and movement in the melt, and internal canister radiant energy transfer. Although such a model offers the potential for a very refined solution, its practical utility is diminished by large computer memory and execution time requirements. On the other hand, the model described in [2] is relatively straight forward in that it predicts temperature and phase distributions in the PCM based solely on conduction heat transfer. PCM container walls and PCM void formation (due to density difference in the PCM solid and liquid phases) are not modeled. This model is used to determine the feasibility and overall performance of a TES device comprised of PCM canisters.

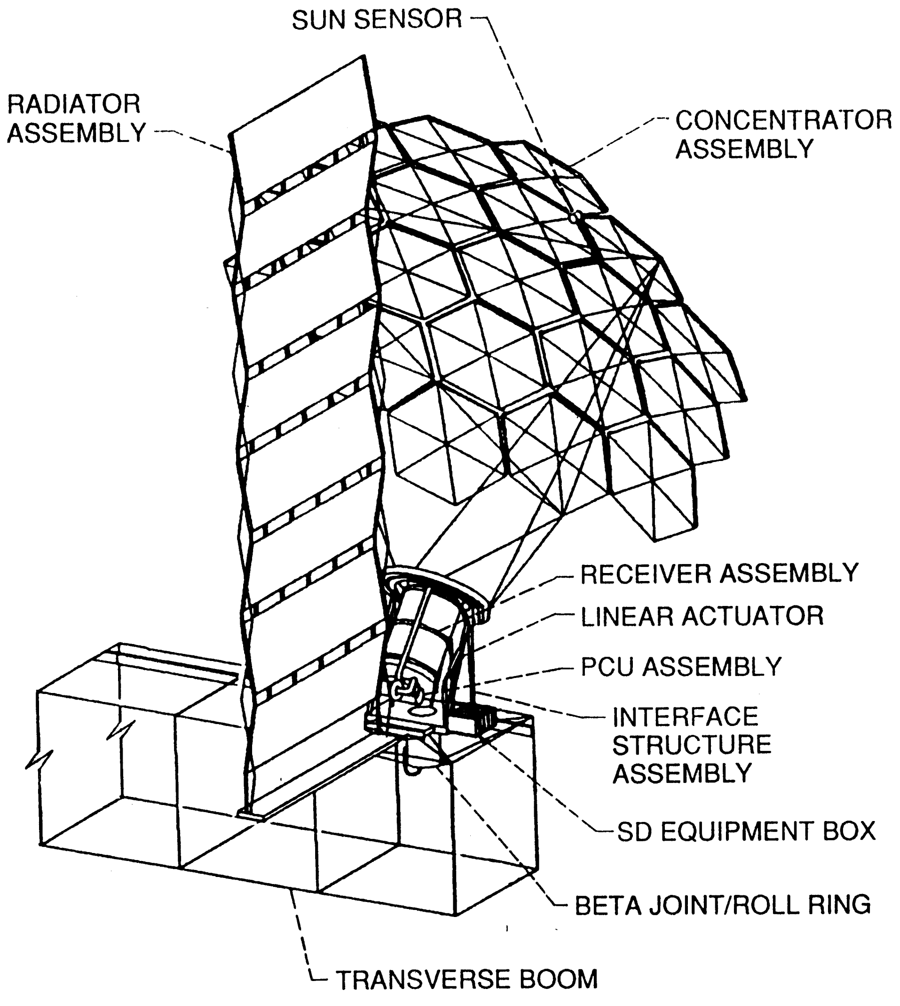

Figure 1. - Closed Brayton cycle solar dynamic power module.

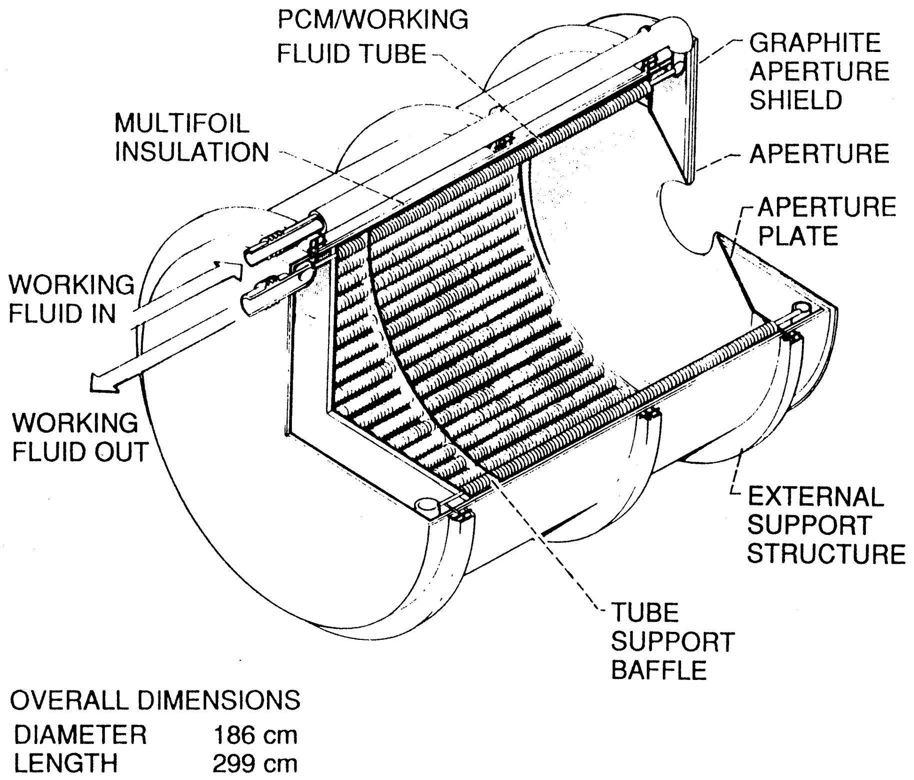

Figure 2. - Heat receiver.

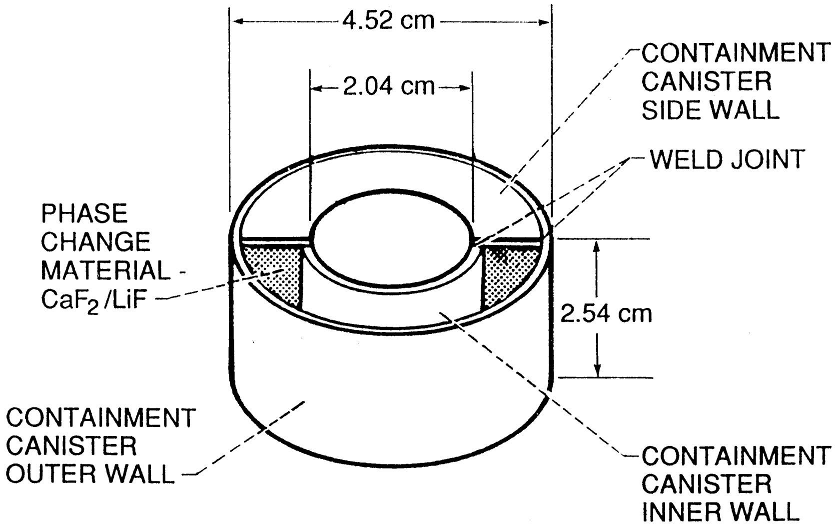

Figure 3. - PCM containment canister (Haynes alloy 188).

A need exists for a "design-oriented" computer model with moderate sophistication to analyze a TES PCM canister. Such a model would have moderate computer memory and run time requirements yet would be capable of multidimensional PCM and containment canister analysis including simplified models of void behavior and liquid salt convection. This type of model could serve as a canister design tool generating detailed temperature distributions for use in structural models and for validating less detailed heat receiver models. In addition this model could address several questions about the canister design that the designer needs to know: How should void heat transfer be modeled? What effect does the void have on canister heat transfer? What are the differences in canister heat transfer during ground tests (in the presence of natural convection) and during flight operation under microgravity conditions?

A moderately sophisticated PCM canister computer model is being developed in three stages considering one-, two- and three-dimensional geometries, respectively. Results from one- and two-dimensional (2D(r,z)) geometries are described in this paper. These geometries are shown schematically in Figure 4. One-dimensional semi-infinite and slab geometries were modeled first because of the relative ease in solving the problem and interpreting numerical results and because of the availability of some exact solutions to verify numerical methods. Further work on two- and three-dimensional models will be reported in the future.

2 ANALYSIS

2.1 Governing Equations

PCM energy redistribution was formulated using "the enthalpy method" described in [3], [4]. Based on conservation of energy, the governing equation is

$$\frac{\partial(\rho e)}{\partial t} + u \bullet \nabla(\rho e) = \operatorname{div}(k \nabla T). \qquad (1)$$

In this equation, e is the specific enthalpy (i.e., given in Joules per gram), u is the void-PCM interface velocity, T is the temperature, ρ is the PCM density, and k is the PCM thermal conductivity. The transport term, $u \bullet \nabla(\rho e)$, is non-zero only for the semi-infinite PCM geometry where void growth during freezing translates the solid PCM region at a rate equal to u. As a simplifying assumption, internal canister radiation terms were not included in the PCM energy balance. Data indicate that mono-crystaline LiF (and presumably liquid LiF) is semi-transparent to radiant energy with wavelengths less than 6.5 μm. Thus, a small fraction of the energy emmitted by internal canister walls will be absorbed within the PCM.

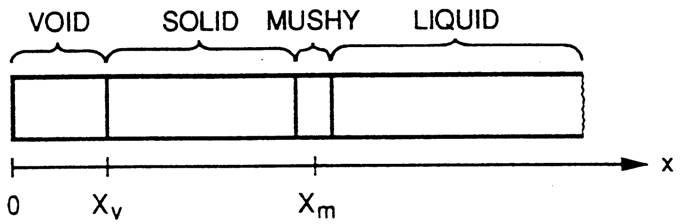

(a) Semi-infinite PCM slab.

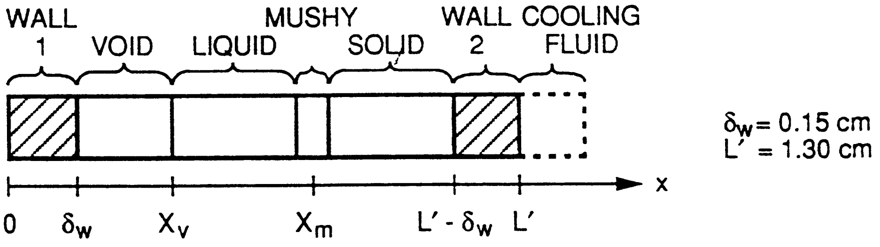

(b) Finite PCM slab canister.

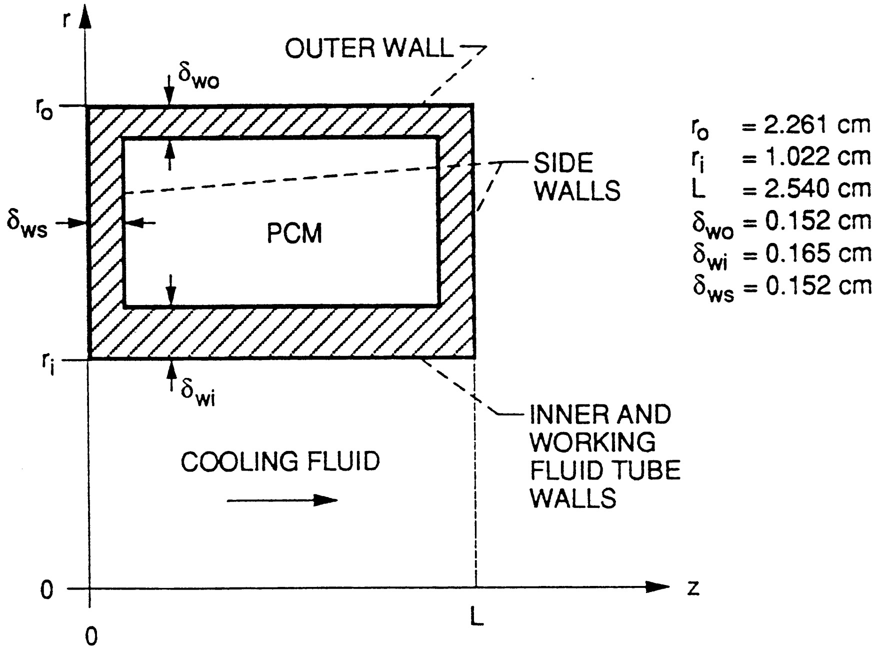

(c) 2D (r,z) PCM canister.

Figure 4. - Schematic problem geometries.

Specific enthalpy is coupled to temperature through the following set of constitutive equations:

$$T = \begin{array}{ll} T_m + e/c_s & : \quad e<0 \\ T_m & : \quad 0 \le e \le H_m \\ T_m + (e-H_m)/c_L & : \quad H_m < e \end{array} \qquad (2)$$

Here, T_m is the PCM melting temperature, H_m is the PCM heat of fusion, and c_S and c_L are the PCM specific heat values in the solid and liquid phases, respectively.

A so-called "mushy" zone exists when $0<e<H_m$. This zone usually consists of dendritic solid phase surrounded by liquid although the exact mushy zone characteristics are functions of material properties, temperature gradients, and interface kinetics [5], [6]. For the purposes of this analysis, mushy zone density and thermal conductivity are treated as linear functions of liquid PCM volume fraction, YF, and mass fraction, XF, such that

$$\rho = (1-YF)*\rho_S + YF*\rho_L \tag{3}$$

$$k = (1-XF)*k_S + XF*k_L \tag{4}$$

where XF and YF are defined as

$$XF = e/H_m \tag{5}$$

$$YF = \{1 + (\rho_L/\rho_S)*(1/XF - 1)\}^{-1} \tag{6}$$

In these equations, the subscripts S and L denote the PCM solid and liquid phases, respectively.

The chief advantage of the enthalpy formulation is that it allows use of a "weak" solution technique, i.e. one that does not require explicit knowledge of solid-liquid phase front location. Instead, phase front location is contained implicitly in the solution since the solid phase exists where $e<0$, liquid phase exists where $H_m<e$, and the approximate phase front location is defined by the mushy phase that exists where $0\leq e\leq H_m$. The formulation also lends itself toward multi-dimensional geometries with periodic boundary conditions that can produce multiple, complex geometry phase fronts.

For the sake of convenience, energy transfer in the PCM containment canister was formulated as in equation (1) using thermophysical properties appropriate for the metallic canister. The constitutive equations in (2) collapse down to the single equation

$$T = T_m + e/c_W \tag{7}$$

where c_W is the canister wall material specific heat.

For one-dimensional PCM geometries, void heat transfer was formulated as conduction, radiation, or conduction plus radiation processes. The void was assumed to be filled with LiF vapor with negligible thermal capacitance and at a pressure equal to the vapor pressure of LiF at 1040 K, i.e. $7\text{x}10^{-3}$ torr. These assumptions seem reasonable since the vapor pressure of CaF_2 at 1040 K is ten orders of magnitude lower than that of LiF [7] and the void vapor mass is small. The void occupied the prescribed regions $0 \le x \le X_v(t)$ and $\delta_w < x \le X_v(t)$ for the semi-infinite PCM slab and finite slab PCM canister models, respectively. Here $X_v(t)$ represents the time dependent location of the void-PCM interface and δ_w represents the thickness of the PCM containment canister wall.

The time dependent void heat flux, q_v, is given by

$$q_v(t) = R_v^{-1} * \{T(0,t) - T(X_v(t),t)\} \tag{8}$$

where R_v is the void thermal resistance equal to $X_v(t)/k_v$ and T is temperature. For a conduction process, the void thermal conductivity, k_v, is equal to the thermal conductivity of LiF vapor, k_{LiFVap}. Using the kinetic theory of gases as in [3], the value of k_{LiFVap} is 4.7×10^{-4} W/cm-K at 1040 K. For a gray radiation process with LiF vapor as a non-participating medium, k_v is given by

$$k_v = \frac{\sigma * X_v(t) * (T(0,t) + T(X_v(t),t)) * (T^2(0,t) + T^2(X_v(t),t))}{(1/\epsilon_W + 1/\epsilon_{PCM} - 1)} \tag{9}$$

where σ is the Stefan-Boltzmann constant, ϵ_{PCM} is the PCM emittance, and ϵ_W is the emittance of the surface or containment wall at x=0. Note, that to be exact for the finite slab geometry, the term T(0,t) must be replaced by $T(\delta_w,t)$ to account for a finite thickness containment canister wall.

Since void conduction and radiation processes are not coupled, superposition is possible. Using the rule of parallel resistances, the effective void thermal resistance from conduction and radiation, $R_{V\ EFF}$, is given by

$$R_{V\ EFF} = \left\{ \frac{k_{LiFVap}}{X_v(t)} + \frac{\sigma * (T(0,t) + T(X_v(t),t)) * (T^2(0,t) + T^2(X_v(t),t))}{(1/\epsilon_W + 1/\epsilon_{PCM} - 1)} \right\}^{-1} \tag{10}$$

It is worth noting that if the void boundaries of interest consist of PCM only, heat transfer across the void via evaporation/condensation can be significant. Scoping calculations have shown that under certain conditions, void heat transfer by radiation and vaporization in a LiF PCM are comparable in magnitude while heat transfer by conduction is an order of magnitude smaller [3].

A simplified description of liquid PCM natural convection based on existing heat transfer correlations was also incorporated into the one-dimensional PCM models. Enhanced heat transfer due to liquid PCM circulation is accounted for by enhancing the value of liquid PCM thermal conductivity, k_L, such that

$$k_{LE} = Nu * k_L \tag{11}$$

where k_{LE} is the enhanced PCM liquid conductivity and Nu is the Nusselt number. This approach was successfully used to predict PCM melt zone height during ground testing of a finned thermal capacitor [8].

For the semi-infinite PCM geometry, a general Nu correlation for a horizontal layer heated isothermally from the bottom was used [9]. The correlation has the form

$$Nu = C5*Ra^{n3} \qquad (12)$$

which is valid for the Prandtl number range $1<Pr<20$. Values for C5 and n3 are given in Table 1. Here the Rayleigh number, Ra, is defined by

$$Ra = \frac{g*\beta*(T(0,t)-T_m)*X_m^3(t)}{\alpha*\upsilon} \qquad (13)$$

where g is gravitational acceleration, $X_m(t)$ is the PCM liquid zone height equal to the characteristic length, and α, β, υ, and T_m are the PCM thermal diffusivity, volumetric thermal expansion coefficient, kinematic viscosity, and melting temperature, respectively.

The Nu correlation used for the finite slab PCM geometry is valid for a vertical layer with isothermal or isoflux heating [9]. It is given as

$$Nu = C5*Ra^{n3}*(LH/w)^{-0.3} \qquad (14)$$

with the restrictions of $1<Pr<20{,}000$ and vertical layer height to width ratio, LH/w, $10<LH/w<40$. Values of the constants are given in Table 1. The Ra number in equation (14) is given as

$$Ra = \frac{g*\beta*(T(X_v(t),t)-T_m)*(X_m(t)-X_v(t))^3}{\alpha*\upsilon} \qquad (15)$$

TABLE 1. - LIQUID PCM NATURAL CONVECTION CORRELATIONS (9)

Geometry	Correlation	c5	n3	LH/w	Ra range
Horizontal layer (semi-infinite slab)	$Nu = c5*Ra^{n3}$	1	0	--	<1700
		0.012	0.6	--	$1.7\times10^3 - 6\times10^3$
		0.375	0.2	--	$6\times10^3 - 3.7\times10^4$
		0.13	0.3	--	$3.7\times10^4 - 10^8$
		0.057	1/3	--	$>10^8$
Vertical layer (finite slab)	$Nu = c5*Ra^{n3}*(LH/w)^{-0.3}$	$0.42\ Pr^{0.012}$	1/4	40	$10^4 - 10^7$

where the characteristic length is the liquid thickness which can be obtained from the difference between the PCM solid-liquid interface and the PCM-void interface, $X_m(t)-X_v(t)$.

2.2 Boundary and Initial Conditions

The boundary and initial conditions for the semi-infinite PCM slab, finite slab PCM canister, and the 2D(r,z) PCM canister problems are contained in Table 2. Exact solutions for the Stefan problem are available for semi-infinite PCM geometries initially at uniform temperature with an imposed constant temperature at one face, i.e. problem numbers 1 and 2 in Table 2 [10], [11]. A specialized exact solution to the Stefan problem with void formation is given in [4].

For the semi-infinite PCM slab problems 1 and 2 in Table 2, the Stefan number (St), defined by $c^*\Delta T/H_m$, was selected to be 0.10. Here ΔT is the absolute value of the difference between initial PCM temperature and the imposed temperature at x=0. This small Stefan number value is representative of phase change processes in TES canisters. For problem 3, the value of q was chosen such that the same amount of PCM energy change occurred as with the constant temperature boundary condition phase change process.

For the finite slab geometry, problem 4, values typical of a LiF-CaF_2 filled TES canister were selected for the length, L', initial temperature, T_s, heat flux input, q(t), film coefficient, h, and cooling fluid temperature, T_f. Values selected also permitted full PCM melting and freezing during the canister simulated charge-discharge cycle.

TABLE 2. - BOUNDARY AND INITIAL CONDITIONS

Problem number	Geometry	Initial condition	Initial PCM phase	Boundary conditions	Exact solution available?
1	Semi-infinite slab	$T(x,0) = T_m$	Liquid	$T(0,t) = T_W < T_m$ $T(\infty,t) = T_m$	Yes
2	Semi-infinite slab	$T(x,0) = T_S < T_m$	Solid	$T(0,t) = T_L > T_m$ $T(\infty,t) = T_S$	Yes
3	Semi-infinite slab	$T(x,0) = T_m$	Liquid	$-k\partial/\partial x[T(0,t)] = q < 0$ $T(\infty,t) = T_m$	No
4	Finite slab	$T(x,0) = T_S < T_m$	Solid	$-k\partial/\partial x[T(0,t)] = q(t)$ $-k\partial/\partial x[T(L',t)] = h[T(L',t) - T_f]$ $h,\ T_f =$ constants	No
5	2D(r,z)	$T(r,z,0) = T_S < T_m$	Solid	$k\partial/\partial r[T(r_o,z,t)] = q(t)$ $k\partial/\partial r[T(r_i,z,t)] = h[T(r_i,z,t) - T_f(z,t)]$ $\partial/\partial z[T(r,0,t)] = \partial/\partial z[T(r,L,t)] = 0$	No

Boundary condition values for the 2D(r,z) canister geometry, problem 5, were based on results obtained from a heat receiver computer model described in [12]. Figure 5 shows the heat input function, q(t), applied to the canister outer surface at $r=r_o$ and the cooling fluid inlet temperature function, $T_f(0,t)$, for a canister located about 115 cm behind the conceptual heat receiver aperture plane. During a simulated 91 minute Space Station Freedom Orbit, canisters in this region of the receiver experience maximum heat input and undergo complete melting and freezing of the PCM. Since adjacent canisters on a given working fluid tube operate at nearly identical temperature, canister side wall boundaries at z=0 and at z=L, the canister length, were treated as adiabatic.

The film coefficient constant, h, was determined based on a correlation discussed in [13] which is valid for fully developed turbulent flow in circular tubes with low Pr number fluids. The heat engine working fluid, a 39.94 molecular weight helium-xenon (He/Xe) mixture, has a Pr of 0.24. The correlation has the form

$$Nu = 0.022*Re^{0.8}*Pr^{0.6} \tag{16}$$

where Re is the Reynolds number. The working fluid mean temperature profile, $T_f(z,t)$, was determined based on a quasi steady state approach.

2.3 Material Properties

For the purpose of this analysis, constant material properties were assumed. These properties are given in Table 3. Note that the LiF-CaF$_2$ PCM and Haynes alloy 188 containment canister material properties were evaluated at 1040 K while the He/Xe working fluid properties were evaluated at 900 K.

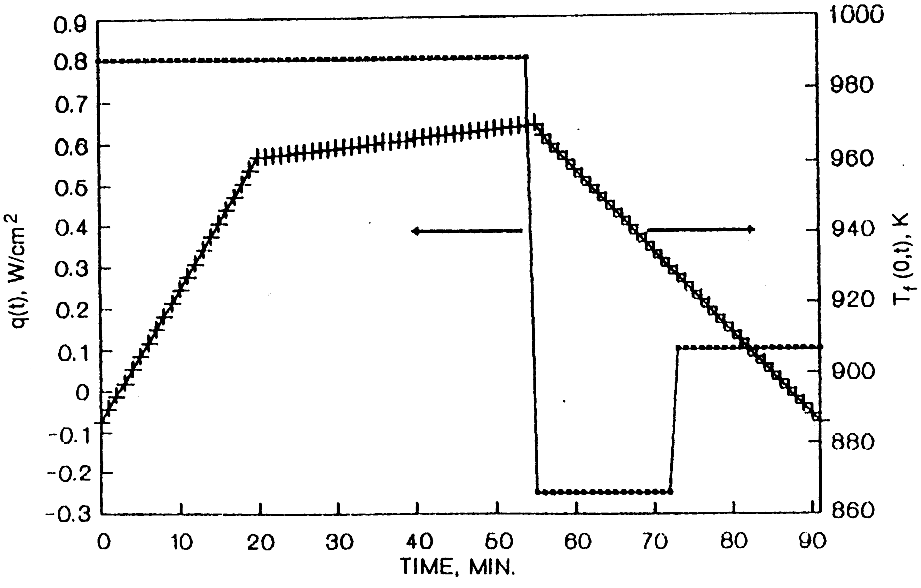

Figure 5. - Boundary conditions for 2D(r,z) model.

TABLE 3. - MATERIAL PROPERTIES

Property	80.5 LiF-19.5 CaF_2 at 1040 K		Haynes alloy 188 at 1040 K	39.94 mol wt He/Xe at 900 K
	Solid	Liquid		
ρ, g/cm3	2.59	2.19	8.813	1.862×10^{-3}
c, J/g-K	1.77	1.77	0.548	0.5202
k, w/cm-K	0.038	0.017	0.246	1.333×10^{-3}
T_m, K	1040		1575 - 1630	----------
H_m, J/g	816		-----------	----------
ν, cm^2/sec	-----	0.0105	-----------	----------
β, 1/K	-----	2.87×10^{-4}	-----------	----------
μ, g/cm-sec	-----	0.023	-----------	5.982×10^{-4}
Pr	-----	2.4	-----------	0.24
ε	0.8	0.8	0.15	----------

2.4 Numerical Method

A simple explicit numerical method was implemented to solve equation (1). On the basis of accuracy, ease of programming, computation time and computer storage requirement, the simple explicit method was ranked third best out of nine numerical schemes used to solve the three-dimensional heat diffusion equation in a parallelepiped [14]. In this study, explicit, implicit, alternating-direction-implicit (ADI), and Crank-Nicolson methods were considered with two similar ADI methods ranking first and second best.

Grid independence tests were performed using the finite slab PCM canister to determine the appropriate grid size for good solution accuracy and resolution. Based on these tests, ~40 grids per cm of PCM was used in one-dimensional models where computation times are small and ~20 radial grids and ~5 axial grids per cm of PCM were used in the 2D(r,z) model to limit computational time.

Because of the time-varying void size in the one-dimensional PCM models, the PCM computational domain, $X_v(t) \le x \le L' - \delta_w$, must be continually up-dated throughout the simulation to avoid the singularity condition in the void region, i.e. mass=0. This was accomplished by calculating the position of $X_v(t)$ based on conservation of PCM mass and by implementing a "combined grid element" technique. This technique simply combines the element that contains the void-PCM interface, iv, with the adjacent element, iv+1, to form one larger element iv′ of width Δx_v given by

$$\Delta x_v = \Delta x^* (1 + MF_v) \qquad (17)$$

where MF_v is the mass fraction PCM contained in element iv at any given time. As the void front translates during the simulation, the value iv will "jump" at discrete instances of time. Once a jump condition has been detected, properties of element iv′ are updated for the future time step based on the average properties of the new elements iv and iv+1 from the current time step.

Based on the local maximum principle discussed in [2], the simple explicit scheme is stable as long as the time step, Δt, is chosen such that

$$\Delta t<\Delta x^2/(2*\alpha) \tag{18}$$

for central PCM grid elements in the one-dimensional PCM canister models and as long as

$$\Delta t< \frac{\Delta r^2/(2*\alpha_w)}{\Psi+\Delta r^2*k_s/(k_s*\delta_{ws}{}^2+k_w*\delta_{ws}*\Delta z)} \tag{19}$$

for canister sidewall grid elements in the 2D(r,z) PCM canister model. In equation (18), Δx is the grid size and α is the PCM thermal diffusity of the solid or liquid phase. This dictates that Δt values less than 0.0375 seconds and 0.0199 seconds must be selected to ensure stability for one-dimensional cases with and without the presence of natural convection, respectively. In equation (19), Δr and Δz are the radial and axial grid spacings and k_w, δ_{ws}, and α_w are the canister sidewall element thermal conductivity, thickness, and thermal diffusivity. The term Ψ is given by

$$\Psi = \frac{\Delta r}{2*r_i}\left\{\frac{1}{\ln(r_{i+1}/r_i)} + \frac{1}{\ln(r_i/r_{i-1})}\right\} \tag{20}$$

where r_i is the radial coordinate of canister sidewall grid element i. This dictates that a Δt value less than 0.0254 seconds must be selected to ensure stability.

Computer programs were coded in FORTRAN 77 and executed on an AMDAHL 5860 computer using double precision variables. Single precision runs were also made to compare run time requirements and accuracy. Single precision runs reduce CPU time requirements by factors of 1.1X and 1.6X for the one and two-dimensional models, respectively. Generally speaking, single and double precision calculations agreed to within 1% for temperature predictions and to within 2-3% for melt front predictions.

3 RESULTS

3.1 Semi-Infinite Slab

Exact and numerical solutions to problems 1 and 2 in Table 2 are shown in Table 4. Numerical melt front solutions are within 0.6%

TABLE 4. - NUMERICAL VERSUS EXACT SOLUTIONS FOR PROBLEMS 1 AND 2

(a) Melt and void front solutions

Time, min	$X_m(t)$, cm						$X_v(t)$, cm	
	Problem 1		Problem 1 with void		Problem 2		Problem 1 with void	
	Numerical	Exact	Numerical	Exact	Numerical	Exact	Numerical	Exact
0.0	0.00000	0.00000	0.00000	0.00000	0.00000	0.00000	0.00000	0.00000
10.0	1.06220	1.07000	0.29491	0.29660	0.44390	0.44430	0.04555	0.04581
20.0	1.50470	1.51320	0.41681	0.41950	0.62587	0.62830	0.06437	0.06479
30.0	1.84420	1.85330	0.50933	0.51380	0.76559	0.76950	0.07866	0.07935
40.0	2.12950	2.14000	0.58637	0.59330	0.88337	0.88860	0.09056	0.09163
50.0	2.37940	2.39260	0.65123	0.66330	0.98732	0.99340	0.10058	0.10244

(b) Temperature solutions

T(x, t = 45 min)/phase											
Problem 1				Problem 1 with void				Problem 2			
x, cm	Numerical	Phase	Exact	x, cm	Numerical	Phase	Exact	x, cm	Numerical	Phase	Exact
0.0000	994.0	SOL	994.0	0.0000	994.0	VOID	994.0	0.0000	1063.0	LIQ	1063.0
0.1125	996.3	SOL	996.2	0.0525	******	VOID	******	0.1125	1060.2	LIQ	1060.2
0.3125	1000.5	SOL	1000.3	0.1104	1037.2	SOL	******	0.2125	1057.7	LIQ	1057.3
0.5125	1004.6	SOL	1004.5	0.1125	******	SOL	1036.6	0.3125	1055.3	LIQ	1055.3
0.7125	1008.7	SOL	1008.6	0.1625	1037.5	SOL	1037.5	0.4125	1052.8	LIQ	1052.9
0.9125	1012.8	SOL	1012.7	0.2125	1037.8	SOL	1037.7	0.5125	1050.3	LIQ	1050.4
1.1125	1016.9	SOL	1016.8	0.2625	1038.0	SOL	1038.0	0.6125	1047.9	LIQ	1048.0
1.3125	1020.9	SOL	1020.8	0.3125	1038.3	SOL	1038.3	0.7125	1045.4	LIQ	1045.6
1.5125	1025.0	SOL	1024.9	0.3625	1038.6	SOL	1038.5	0.8125	1043.0	LIQ	1043.1
1.7125	1029.0	SOL	1028.9	0.4125	1038.9	SOL	1038.8	0.9125	1040.5	LIQ	1040.7
1.9125	1032.9	SOL	1032.9	0.4625	1039.2	SOL	1039.1	0.9625	1039.9	SOL	1039.9
2.1125	1036.9	SOL	1036.9	0.5125	1039.4	SOL	1039.4	1.0125	1039.8	SOL	1039.8
2.2125	1038.9	SOL	1038.9	0.5625	1039.7	SOL	1039.6	1.0625	1039.6	SOL	1039.7
2.3125	1040.0	MUSH	1040.0	0.6125	1040.0	MUSH	1039.9	1.1625	1039.4	SOL	1039.4
2.4125	1040.0	LIQ	1040.0	0.6625	1040.0	LIQ	1040.0	1.2625	1039.1	SOL	1039.2

of the exact solutions without voids and within 1.8% of the exact solution with void. Numerical temperature solutions are within 0.5 K of the exact solutions for all problems. These results indicate that the numerical scheme is fairly accurate and properly implemented.

The effect of a void on the PCM freezing process of problem 2 is evident in Figure 6 which illustrates $X_m(t)$ versus t for cases with and without a void. Here, the presence of the void reduced the amount of PCM frozen by 72% and 79% assuming void heat transfer via conduction and radiation, respectively. For small St number freezing processes, the amount of energy removal is essentially proportional to the amount of PCM frozen. Therefore, in this case where void size is small (i.e., 15% of $X_m(t)$), the magnitude of void heat transfer via conduction and radiation are comparable.

The effect of boundary conditions on the freezing processes in problems 1 and 3 can be seen in the plots of boundary temperature and freeze front location versus time shown in Figures 7 and 8,

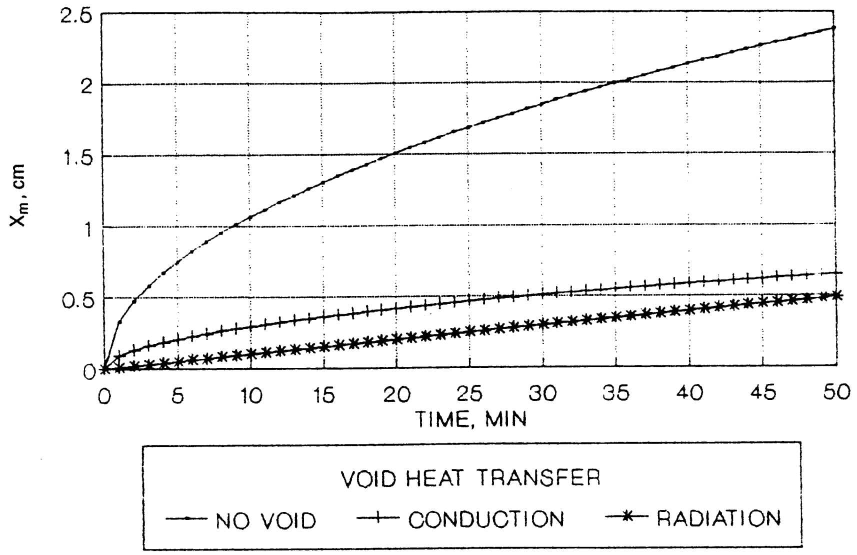

Figure 6. - Melt front location for freezing process with St = 0.10.

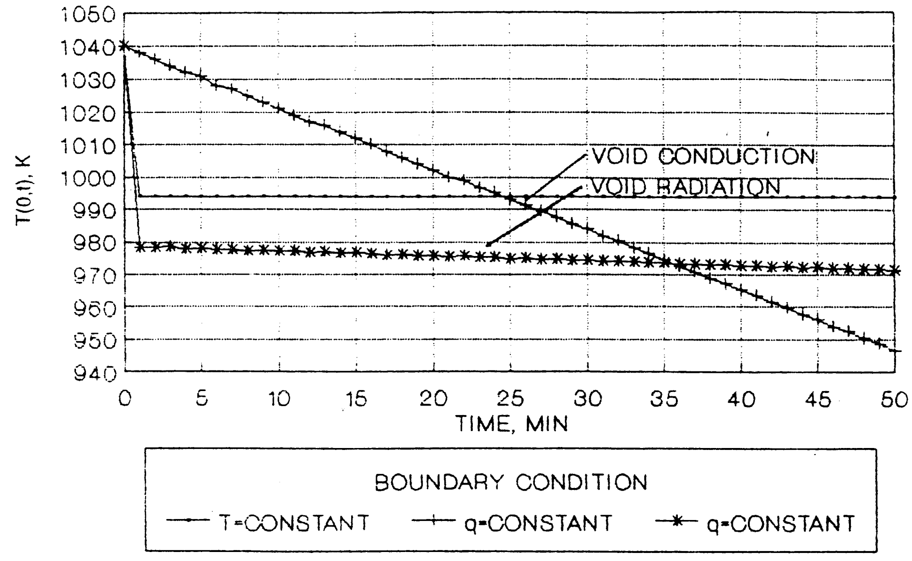

Figure 7. - Boundary temperatures for equal energy removal processes.

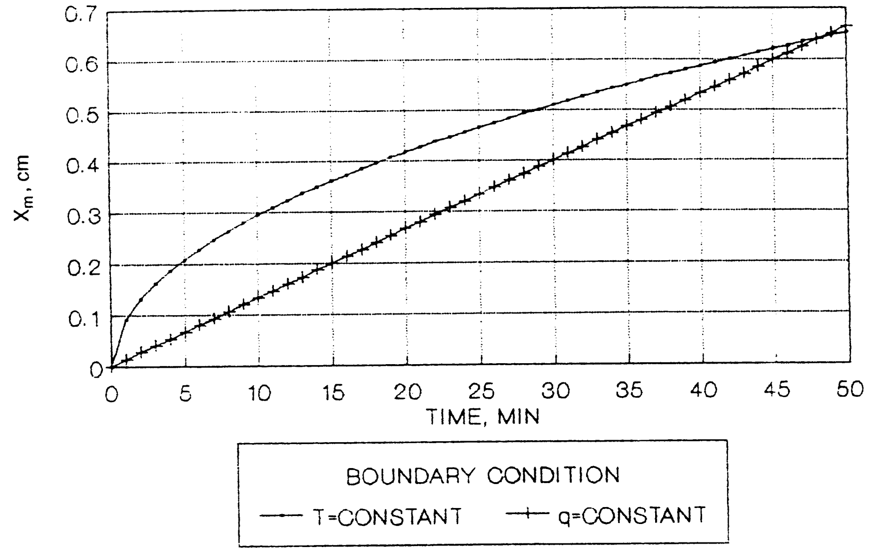

Figure 8. - Melt front locations for equal energy removal processes.

respectively. In all cases, comparisons between constant temperature and constant heat flux boundary conditions were made on the basis of equal energy removal. Boundary temperature, T(0,t), decreases linearly versus time with constant wall heat flux (see Figure 7). However, with radiation void heat transfer, variation in T(0,t) is small. This confirms the insensitivity of radiation heat transfer to void size. Freeze front advancement differs substantially with boundary condition assuming conduction void heat transfer (see Figure 8). A constant temperature boundary condition initially generates high PCM freezing rates and temperature gradients which decrease quickly while a constant PCM freezing rate and temperature gradient exist with constant wall heat flux.

The effect of natural convection on a melting process with St=0.10 is illustrated in Figure 9. Figure 9 contains plots of $X_m(t)$ versus t, T(x, 25 min) versus X, and q(0,t) versus t for cases with and without natural convection present. Although constant temperature is maintained x=0, the progression of $X_m(t)$ is nearly linear (see Figure 9a). This is characteristic of a constant heat addition melting process. The presence of natural convection also increases the amount of PCM melted at t=50 minutes by a factor of 2.68X. At this point in time, the liquid PCM Nu number is about 11 and steadily increasing. At t=25 minutes, temperature gradients in the liquid PCM are reduced by a factor 2X while at the same time the wall heat flux, q(0,25 min), is increased by ~3X (see Figures 9b and 9c). The local peak in the q(0,t) curve for the case with natural convection corresponds to the point in time when the product of Nu*(∂T/∂x@x=0) is greatest. For $Ra>10^5$, Nu increases linearly with $X_m(t)$. This implies that the natural convection film coefficient is independent of $X_m(t)$.

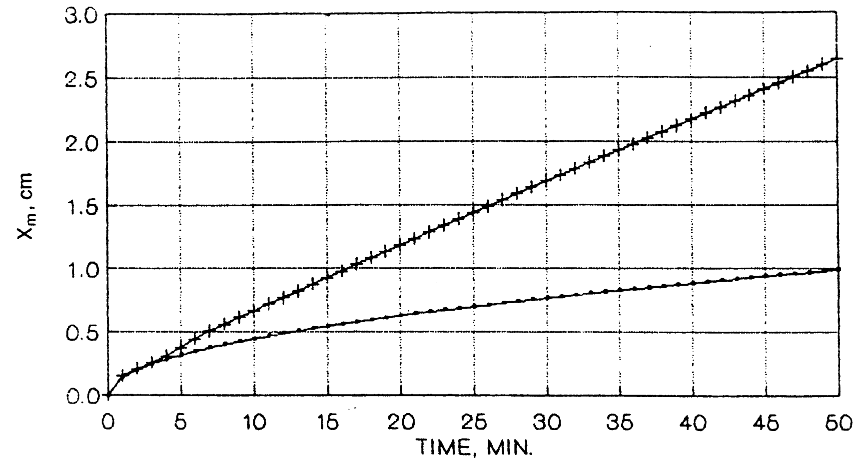

(a) Melt front location.

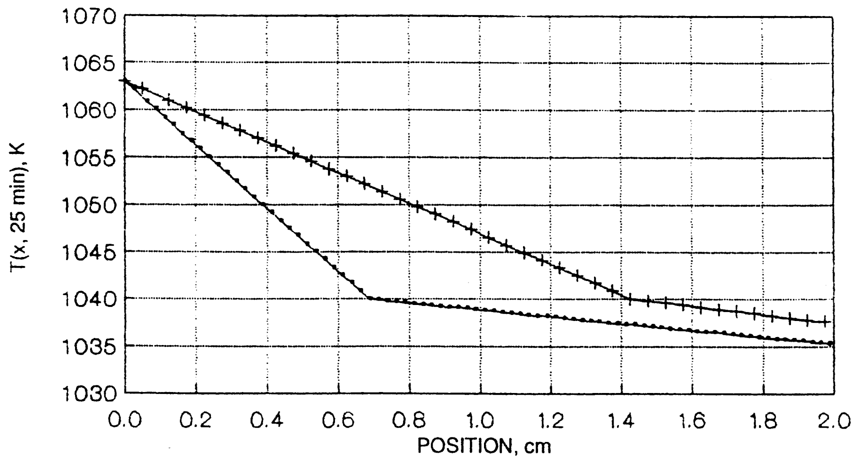

(b) PCM temperature distributions.

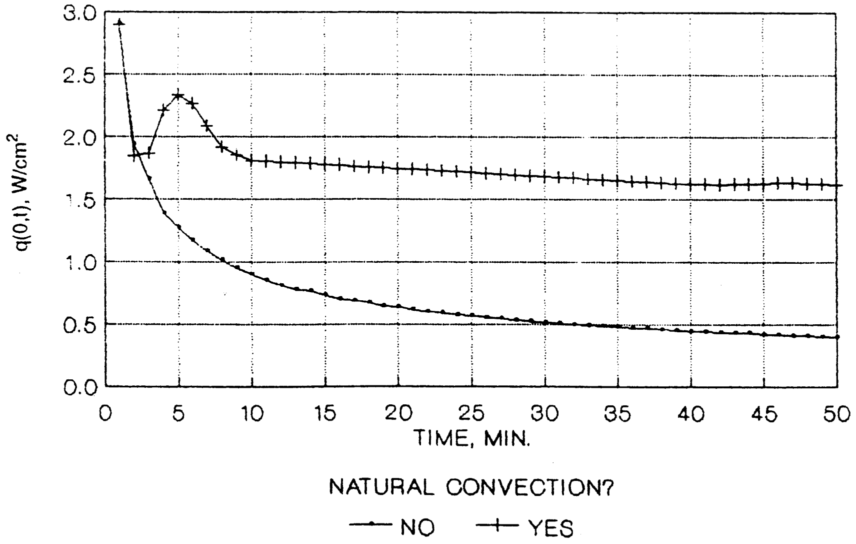

(c) Boundary heat flux.

Figure 9. - Problem 2 with St = 0.10.

ORIGINAL PAGE IS
OF POOR QUALITY

3.2 Finite Slab

Void thermal resistance is plotted as a function of time in Figure 10 for a representative size finite slab PCM containment canister undergoing a 30 minute, constant heat input melting period and a 20 minute, zero heat input freezing period.

Conduction and radiation thermal resistances are of the same order of magnitude and both vary significantly with time due to variations in void size and canister wall temperature, respectively. Therefore, void heat transfer is most accurately modeled as a simultaneous conduction-radiation process with the resultant thermal resistance shown in Figure 10. The canister wall 1 temperature, T(0,t), is shown in Figure 11. Heat input to the canister is applied at wall 1 which is adjacent to the void while wall 2 is convectively cooled by the heat engine working fluid (see Figure 4). T(0,t) predictions widely vary depending on the assumed type of void heat transfer. With combined mode void heat transfer, T(0,t) is nearly isothermal at 1290 K during melting and at 1050 K during freezing.

Figure 12 illustrates the impact of natural convection on PCM melt and void front positions, canister wall temperatures and PCM temperature distributions. The PCM occupies the region $0.15<x<1.15$ cm between the two canister walls while the void occupies the region $0.15<x\lesssim0.30$ cm as it grows and shrinks due to density differences in the solid and liquid PCM. Little difference exists between melt/void front locations with the addition of natural convection (see Figure 12a). However, the presence of natural convection significantly lowers canister wall 1 temperatures and PCM temperature gradients during the TES charge period in addition to melting slightly more PCM (see Figures 12b and 12c).

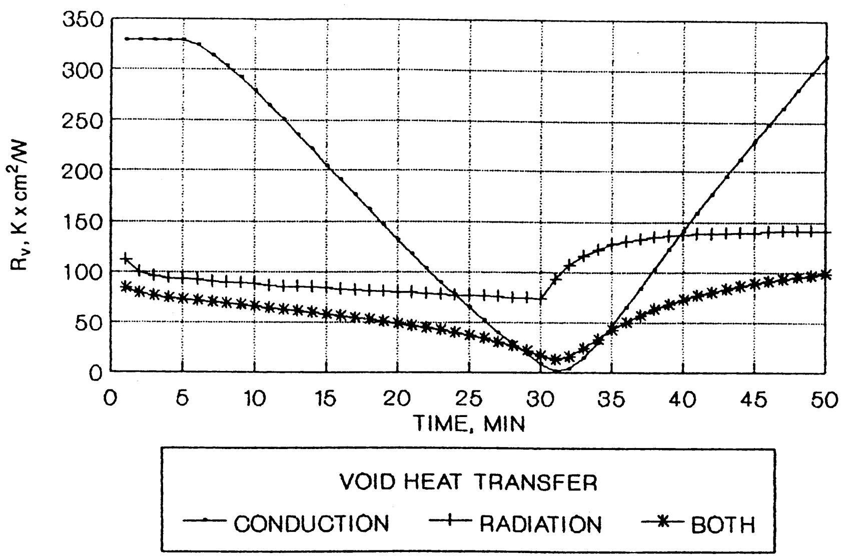

Figure 10. - Void thermal resistance.

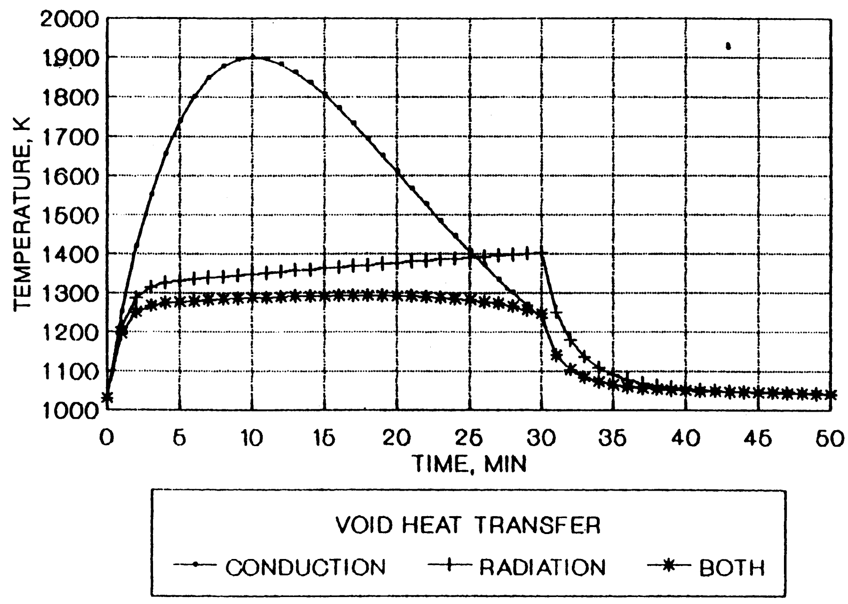

Figure 11. - Wall 1 temperature.

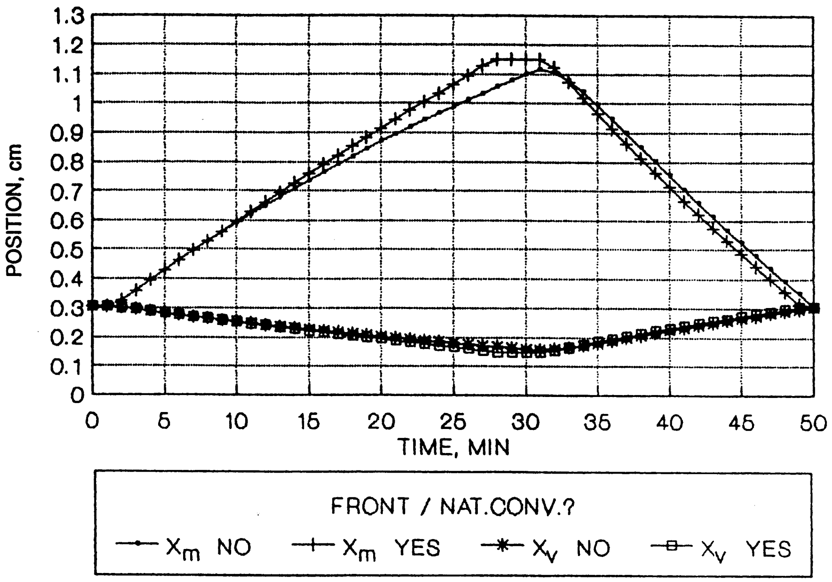

(a) Melt and void front positions.

Figure 12. - Finite slab canister results.

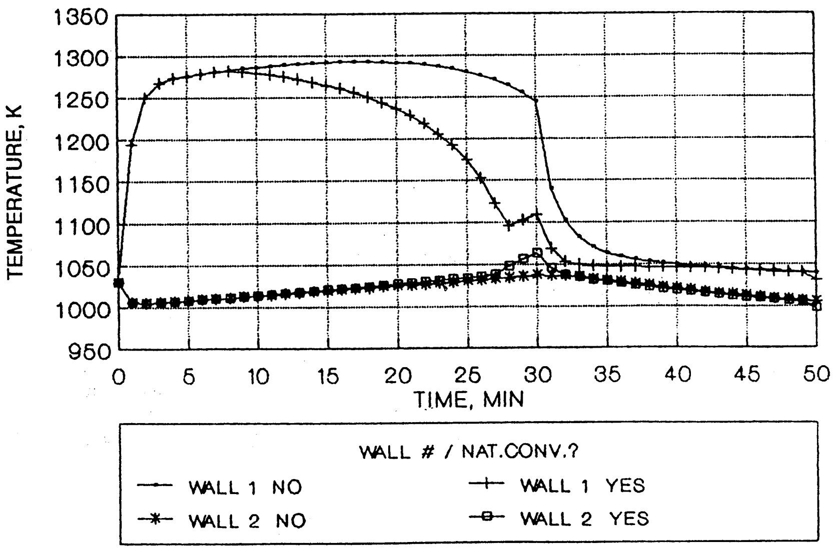

(b) Wall temperatures.

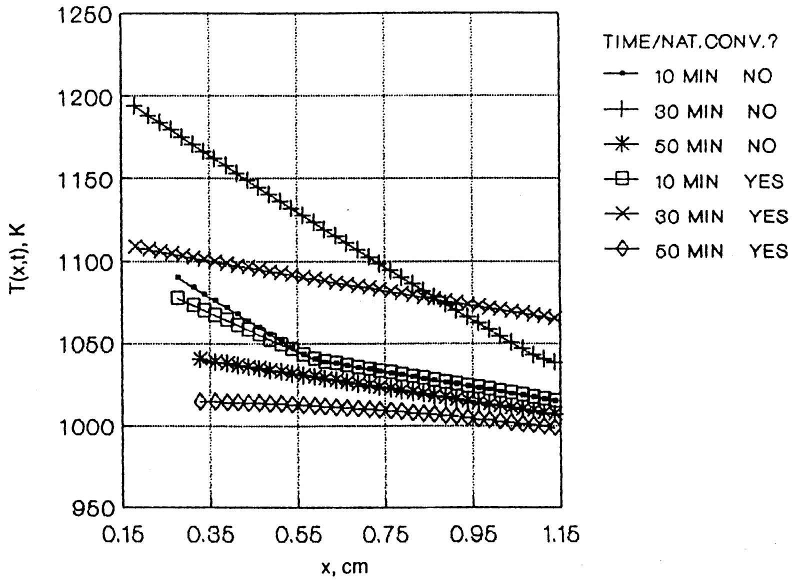

(c) PCM temperature distributions.

Figure 12. - Finite slab canister results.

Figure 13 shows the liquid PCM Nu as a function of melt front position X_m. After exceeding the critical Ra at $X_m \approx 0.50$cm, the Nu increases linearly with X_m until a complete PCM melt has occurred. At this point, Nu≈3.4 which is about 35% lower than Nu for the semi-infinite slab with the same X_m. This seems reasonable since the heat input is applied to the bottom of the semi-infinite slab resulting in greater convective instability than with the finite slab that is heated from the side. During freezing, Nu falls off rapidly and becomes linear with a slope about 25% lower than during melting. This is attributed to

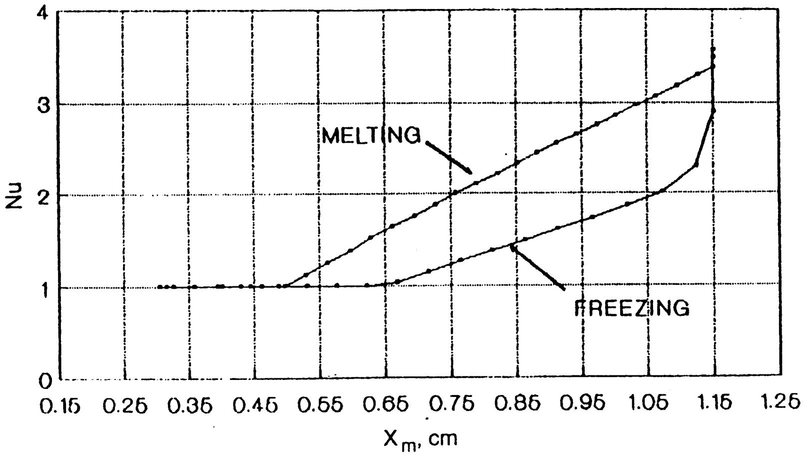

Figure 13. - Nusselt number versus melt front position.

smaller Ra numbers resulting from reduced temperature gradients. This suggests that h is essentially independent of X_m but is a function of melting and freezing.

Since the void in actual PCM containment canisters is not evenly distributed around the circumference [15], the behavior of localized canister radial segments can roughly be approximated by the behavior of one-dimensional PCM models with or without a void. Figure 14 illustrates wall 1 temperature predictions for cases with and without a void. The void increases wall 1 temperatures between 50-200 K throughout the TES charge period with constant heat input. This introduces the potential that for PCM canisters with asymmetric heat input, the maximum wall temperatures will not occur at the point of maximum heat input but instead will occur in the region of the void. Hence, the position of the void must be quantified to accurately

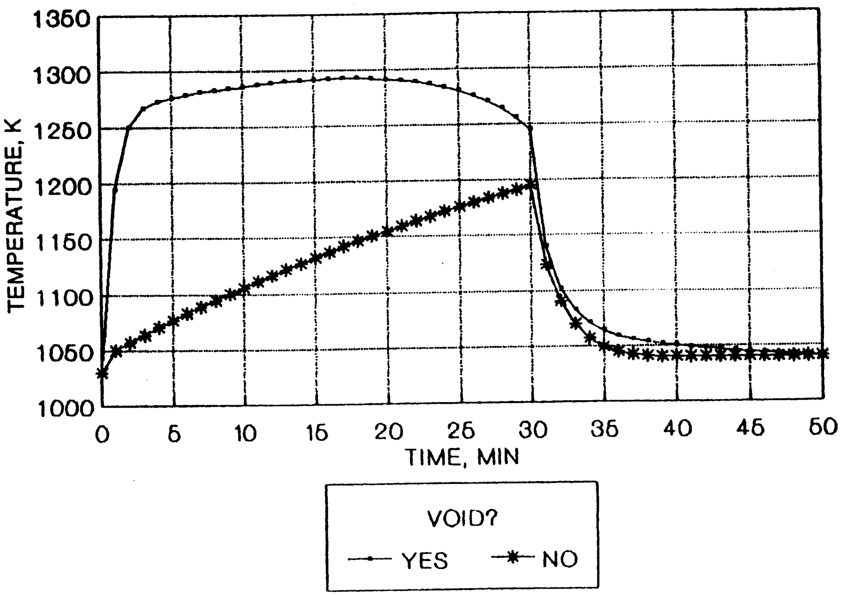

Figure 14. - Wall 1 temperatures.

characterize wall temperatures of canisters with high length-to-diameter ratio, i.e. canisters with small sidewall end effects. Accurate prediction of the void location requires complex calculations and several assumptions. A more straight-forward approach is to place the void along the heat input surface to yield conservative temperature predictions. It will be shown later with 2D(r,z) canister model results that for low length-to-diameter ratio canisters, i.e. $l/d<1.0$, wall temperature sensitivity to void location is greatly reduced because of the large heat transfer contribution of canister sidewalls.

Figure 15 illustrates Nu versus X_m for cases with and without a void. Note that the effects of natural convection are accentuated for the case with no void. TES charge period Nu numbers are higher and TES discharge period Nu numbers are lower than those occurring with the void. These results can be ascribed to differences in characteristic length and temperature gradient between the two cases. In the no void case, the liquid PCM occupies a larger volume, and thus has a larger characteristic length, over that of the void case. Temperature gradients in the case with void are smaller than those of the no void case since the large void thermal resistance reduces the extent of liquid PCM super-heating.

3.3 2D(r,z) Canister

To assure proper implementation of the numerical equations, the 2D(r,z) canister computer model was exercised independently in the r and z coordinate directions and the results were compared to the exact solution of problem 2 in Table 2. Numerical and exact solutions agreed to within 0.6%. In addition, the computer model global energy balance was checked to assure that boundary conditions were properly implemented. An energy balance was maintained to within 0.003 percent.

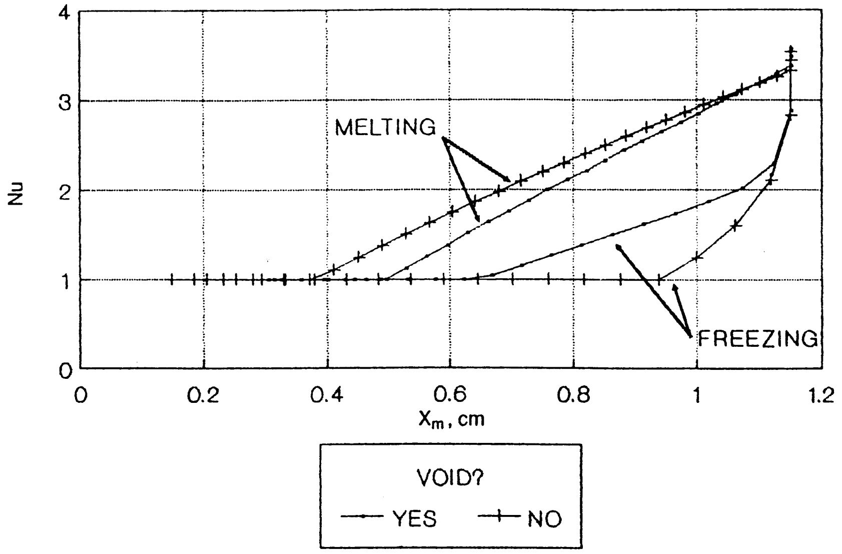

Figure 15. - Nusselt number versus melt front position.

PCM phase distributions are shown in Figure 16 at several points in time (24.28, 54.63, 66.77, and 91.05 minutes) for a 91 minute cycle in which the PCM is being charged for the first ~55 minutes and discharged for the remaining ~36 minutes. The heat transfer benefits of the canister sidewalls is evident at 24.28 minutes into the TES charge period. The liquid and mushy PCM regions extend radially inward adjacent to canister sidewalls to a greater extent than the bulk PCM. This indicates the manner in which sidewall heat transfer enhances PCM melting in both radial and axial directions without the need for large liquid PCM temperature gradients. Nearly complete PCM melting occurs by 54.63 minutes at which time only a small mushy region exists at the canister inner radius.

At 66.77 minutes, mushy PCM and solid PCM regions completely surround a liquid PCM core region. This phase distribution is the result of heat removal at both inner and outer radial canister surfaces during the first half of the TES discharge period. As freezing continues, the solid region growths inward from all sides until the liquid core region ceases to exist about 6 minutes prior to the end of the discharge period. Thus, at 91.05 minutes, only solid PCM exists. This kind of freezing process suggests that had PCM density differences been accounted for, the resultant void volume would most likely end up as a central core region surrounded by solid PCM. Observations of ground based canister PCM distributions tend to confirm this assertion [15].

Canister temperature contour maps that correspond to the PCM phase maps are shown in Figure 17. The detailed isotherms reveal the approximate distribution of PCM. Noticeable isotherm compression occurs in the vicinity of the melt front as evidence of the relatively high heat transfer rates needed to support PCM melting (see Figure 17a) or PCM freezing (see Figure 17c). At times when only liquid PCM or only solid PCM exists, isotherms are spaced in a relatively uniform fashion (see Figures 17b and 17d, respectively). Noticeable bending in the isotherms occurs near canister walls. This illustrates the effect of canister wall heat transfer enhancement that effectively behaves as a heat sink for the outer wall and as a heat source for the inner wall.

Figure 18 illustrates the variation in maximum canister wall temperature and heat transfer to the cooling fluid as a function of cycle time. Maximum wall temperature occurs at the outer radius, $z=L/2$ and is a strong function of the phase change process (see Figure 18a). As long as liquid and solid PCM coexist (in this case from 9-86 minutes), wall temperatures will not strongly deviate from the PCM critical temperature, T_m. However, once a single PCM phase exists, large temperature transients result as a consequence of sensible energy change.

Variation in cooling fluid heat transfer can generally be ascribed to variation in cooling fluid inlet temperature, $T_f(0,t)$ (see Figure 18b). Heat transfer to the fluid is proportional to

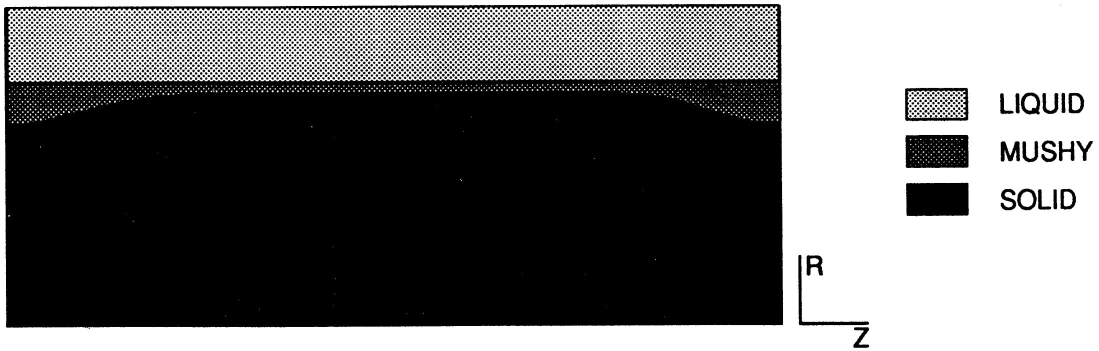

(a) Time = 24.28 min, MFL = 0.30.

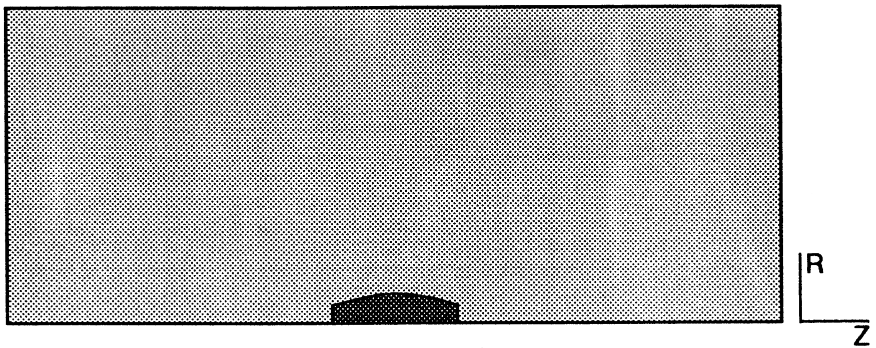

(b) Time = 54.63 min, MFL = 0.99.

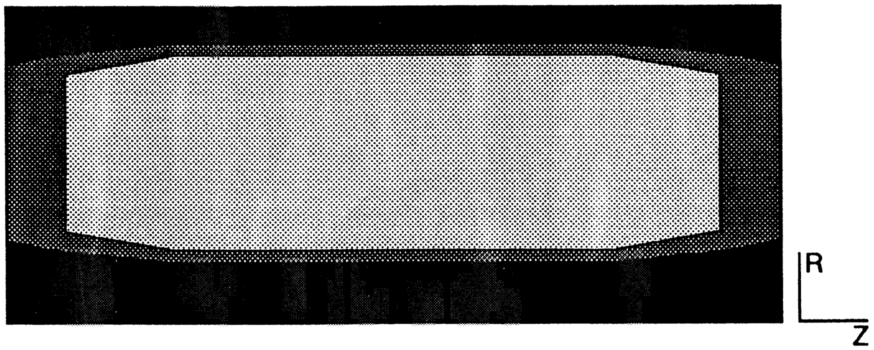

(c) Time = 66.77 min, MFL = 0.63.

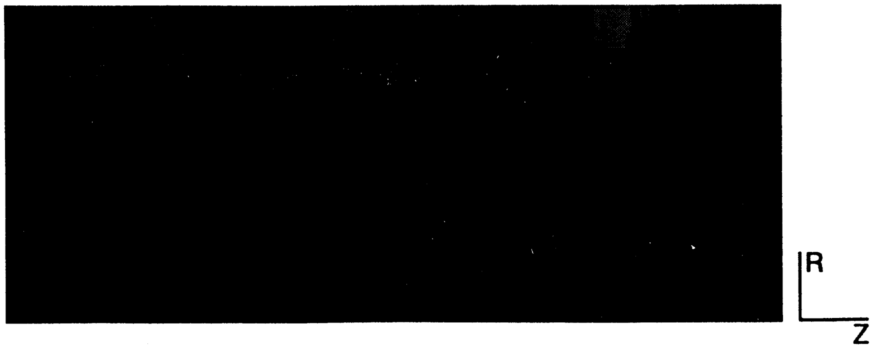

(d) Time = 91.05 min, MFL = 0.00.

Figure 16. - PCM phase maps.

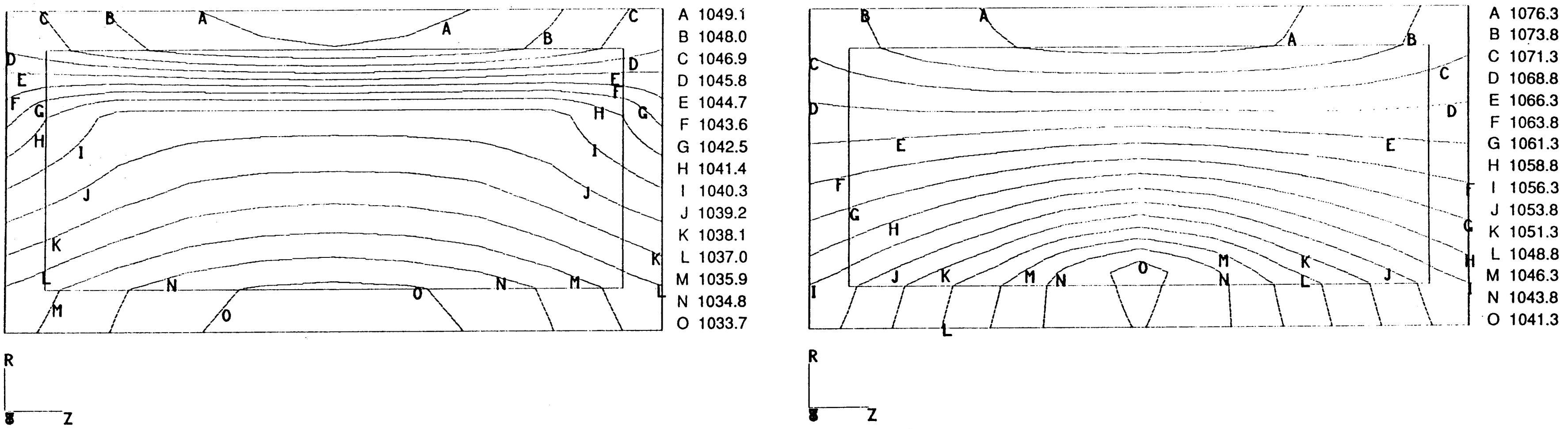

(a) Time = 24.28 min.

(b) Time = 54.63 min.

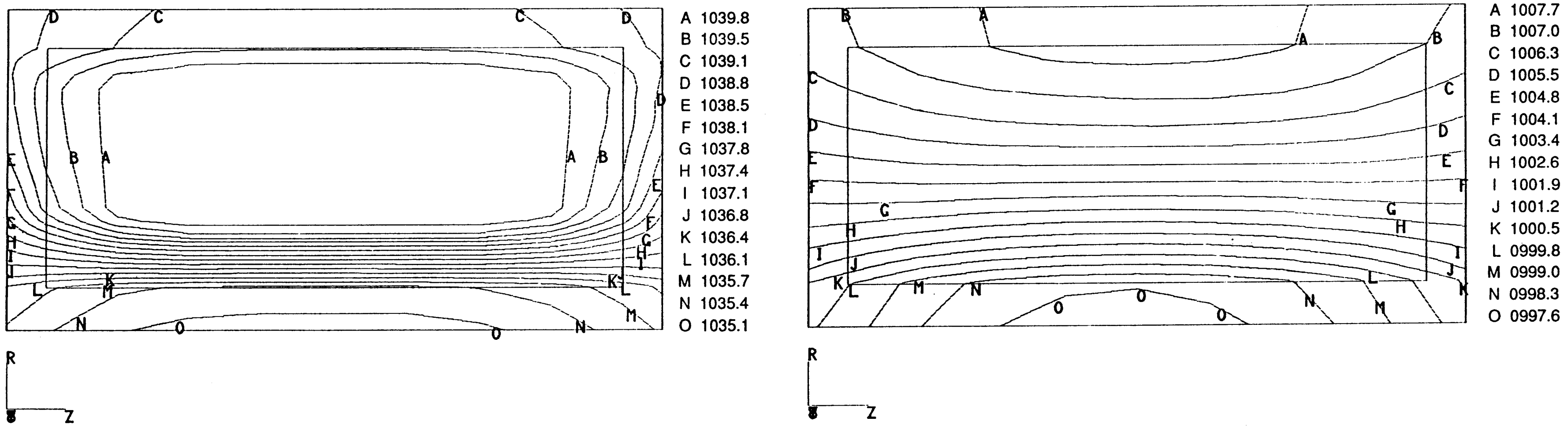

(c) Time = 66.77 min.

(d) Time = 91.05 min.

Figure 17. - Canister temperature contour maps, K.

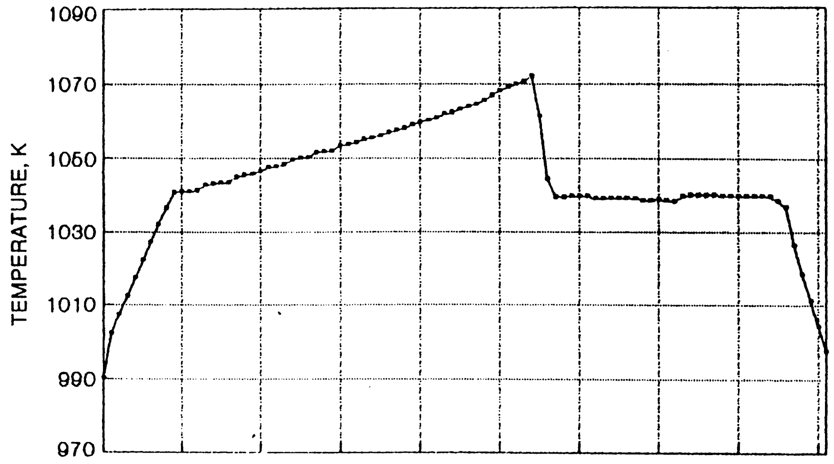

(a) Maximum canister wall temperature.

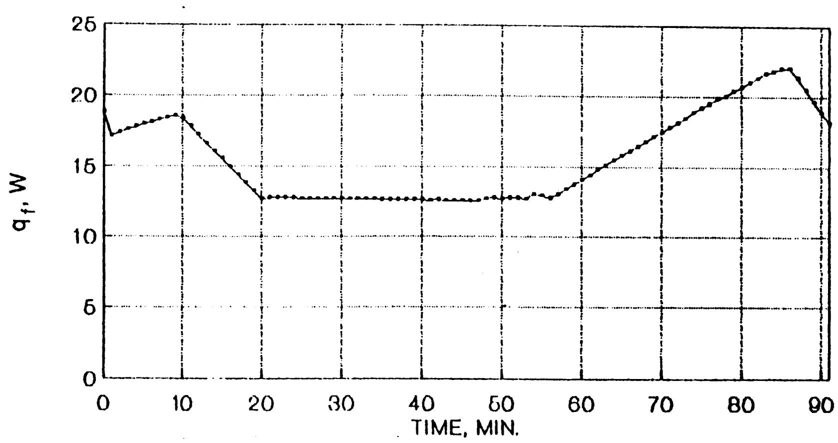

(b) Heat transfer to cooling fluid.

Figure 18. - Cyclic variations in maximum canister wall temperature and heat transfer to the cooling fluid.

the temperature difference between the canister tube wall and fluid. Since most of the cycle time two-phase PCM exists, canister tube wall temperatures remain fairly constant near T_m. Thus, fluid heat transfer decreases as $T_f(0,t)$ increases and increases as $T_f(0,t)$ decreases. The exception to this behavior occurs at the beginning and at the end of the 91 minute cycle when only solid PCM exists. During these periods, canister tube wall temperatures increase toward or decrease from $\sim T_m$ faster than the variation in $T_f(0,t)$ during the beginning and end of the cycle, respectively. This causes the fluid heat transfer to increase and decrease with increasing and decreasing $T_f(0,t)$, respectively.

Since the LiF-CaF_2 PCM is a poor thermal conductor, highly conducting canister walls are necessary to distribute energy absorbed at the canister outer surface to the PCM and to the cooling fluid (heat engine working fluid) without excessive temperature gradients. One measure of the effectiveness in which the canister walls redistribute absorbed energy is the fraction of total canister radial heat transfer which occurs via the canister sidewalls. This "sidewall fraction" is plotted versus time in Figure 19 for three radial locations: r_i^+, r_o^-, and $(r_i + r_o)/2$. Sidewall fractions generally run between 40% and 60% during the heat input period. Three distinctive dips in the curves are evident at times 12 minutes, 32 minutes, and 53 minutes for locations r_o^-, $(r_i + r_o)/2$, r_i^+, respectively. These dips are associated with the passage of the PCM melt front at which time radial PCM heat flow increases (thereby decreasing the sidewall fraction) to support the melt front advancement.

During the heat removal period, sidewall fractions are widely varying. The sidewall fraction at r_o^- closely follows the variation in boundary heat flux, q(t). Initially, q(t) is negative which effectively flattens canister sidewall radial temperature gradients near the outer radius causing the sidewall fraction to approach zero. At 73 minutes, q(t) becomes positive and quickly re-establishes sidewall temperature gradients forcing the sidewall fraction up into the 70% - 100% range. The opposite behavior occurs at $(r_i + r_o)/2$ which is the canister mean radius. As shown by Figure 16 at 66.77 minutes, a small liquid PCM zone surrounded by solid and mushy PCM exists in the central portion of the canister volume. Radial temperature gradients through this liquid zone are small giving rise to 99% wall fractions through the 71 minute point in the cycle. Thereafter, the PCM freeze front advances radially outward beyond $(r_i + r_o)/2$ establishing larger solid PCM temperature gradients in response to cooling fluid heat extraction at r_i.

4 DISCUSSION

Semi-infinite slab results for different boundary conditions indicate that a constant temperature heat sink (or heat source),

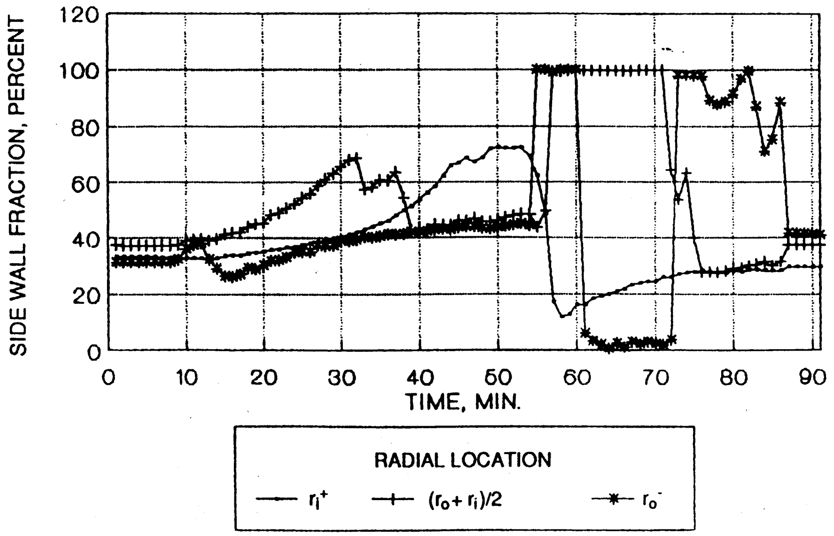

Figure 19. - Fraction of total canister radial heat transfer through side walls.

such as a nearly isothermal heat pipe, maintains the boundary temperature closer to T_m than does a constant flux heat sink. The practical implication of this result is that lower PCM containment wall temperatures will occur with a heat pipe receiver concept versus a direct absorption receiver concept. Keeping canister wall temperatures close to T_m is important for achieving a 30 year service life since increasing temperature enhances the PCM corrosion rate and reduces canister material strength. However, the benefit of lower canister wall temperatures must be weighed against the added complexity and mass of a heat pipe receiver concept.

Results from the finite slab PCM canister indicate that void heat transfer is best modeled as a combined conduction-radiation process. Ignoring the conduction component of void heat transfer increases canister wall 1 temperature predictions by 50 to 150 K over those with combined mode void heat transfer. Note that canister heat input is applied at wall 1 which is adjacent to the void (see Figure 4). This magnitude of temperature difference is probably not acceptable since it would lead to an overly conservative canister design. Ignoring void radiation results in wall 1 temperatures that exceed the melting range of Haynes alloy 188 (1575 to 1630 K). In all cases, wall 1 temperature predictions are too high for long term operation of containment canisters constructed with superalloys. This illustrates the need for heat transfer enhancement fins between heat addition and heat removal surfaces when dealing with low conductivity PCM's to limit maximum wall temperatures to ~1120 K.

It should be noted that one-dimensional canister analysis accentuates wall temperature increases introduced by a void since all canister absorbed energy must be transferred across the void. In an actual canister, absorbed energy in the outer wall has multiple heat transfer paths in which to diffuse. Thus, wall temperature increases due to the presence of a void would be much less pronounced than indicated from one-dimensional predictions. The sensitivity of wall temperatures to void location and to the nature of void heat transfer depends on the extent to which PCM heat transfer is required for energy redistribution within the canister. Figure 19 shows that during the cycle heating period, when highest canister wall temperatures exist, about 40%-50% of canister total radial heat transfer occurs through side walls. This suggests that the sensitivity of canister wall temperatures to PCM-void distribution is greatly reduced over the one-dimensional case. The magnitude of this reduction may render void heat transfer secondary in importance to canister and PCM heat conduction/convection. In this case, wall temperature predictions would be essentially independent of the method used to model void heat transfer. Results from steady state PCM canister heat transfer analyses discussed in [16] support this assertion. Here maximum canister wall temperature increased by only 29 K with the addition of a circumferential void at the canister outer diameter.

Although the effect of a given void on transient canister wall temperatures has not been quantified with the 2D(r,z) model, the extreme case of a canister filled with PCM of zero thermal conductivity was run to determine the upper limit of canister wall temperatures. For this case, peak canister wall temperature runs between 20 K and 135 K higher than what is predicted for the canister with finite conductivity PCM. The likely peak wall temperature for a canister containing PCM with a void will be somewhere in between the predictions of these two cases. Quantitative wall temperature predictions will be available in the next stage of 2D(r,z) PCM canister computer model development when PCM volume change and natural convection effects are incorporated.

Several comments can be made about the effects of liquid PCM natural convection and its implications for ground-based testing of the conceptual heat receiver or PCM containment canisters designed for operation in low earth orbit. Analyses have shown that liquid PCM convective flows arising from buoyancy and surface tension forces are small in a microgravity environment. Thus, liquid PCM heat transfer during on-orbit operation will take place primarily via thermal conduction.

The obvious effects of natural convection, based on one-dimensional analysis, are lower canister wall temperatures and increased PCM melting rate during heat input periods. During thermal discharge periods, natural convection effects are small. Effects during heat input periods are enhanced for the configuration in which canister heat input is from the bottom as opposed to heat input from the side.

These results suggest that canister ground tests should be conducted with heat input on the canister top or side surfaces to minimize natural convection effects. The preferred heat receiver ground test orientation should be with the axis of the receiver vertical. This orientation permits canisters on each working fluid tube to be heated from the side thereby experiencing uniform natural convection effects. A test conducted with the receiver axis horizontal would cause canisters on top receiver tubes to be heated from the bottom while canisters on bottom tubes would be heated from the top. This situation would skew tube-to-tube canister performance and introduce additional receiver cavity circumferential temperature variations not expected during on-orbit operation.

It is difficult to quantify the effects of canister liquid PCM convection on receiver cavity heat transfer which in turn determines canister heat input boundary conditions. However, it can be stated that natural convection effects during ground tests will improve heat receiver performance over that expected during on-orbit, micro-gravity operation. Improvements will include lower canister wall temperatures in high heat input regions of the heat receiver, higher overall PCM utilization, greater receiver cavity isothermallity, and lower receiver heat losses.

The effects of PCM voids and natural convection on containment canister thermal performance will be better understood in the near future as more capability is added to the 2D(r,z) canister computer model described in this paper. In addition, canister thermal cycling tests are currently be conducted at NASA-Lewis Research Center as part of the Space Station Freedom Work Package 4 Supporting Development Program. Data generated from these tests should prove extremely valuable in correlating numerical results and in understanding the complex heat transfer taking place within the PCM canister.

5 SUMMARY OF RESULTS

The results of the numerical study of one- and two-dimensional PCM containment canisters are summarized below as:

1. The numerical models developed accurately predict PCM canister thermal performance with and without the inclusion of a void (on the basis of exact solutions).

2. For a given TES requirement, a constant charge/discharge boundary temperature results in lower boundary temperature variations from T_m than with a constant flux boundary condition.

3. One-dimensional void heat transfer from canister wall to PCM is best modeled as a combined conduction-radiation process. It is conjectured that the choice of void heat transfer model for two-dimensional analyses is much less important due to the large heat transfer contribution of canister walls.

4. The presence of a one-dimensional void substantially reduces material phase change rate under constant temperature boundary conditions and substantially increases canister wall temperatures under constant flux input conditions. As an extreme upper limit, wall temperature increases from a two-dimensional void are about half as much as those from a one-dimensional void. Actual temperature increases are expected to be much less.

5. Based on the two-dimensional PCM freezing process, a central core void location completely surrounded by solid PCM is anticipated at the end of the discharge period when PCM density change is accounted for.

6. The presence of liquid PCM natural convection significantly lowers canister wall temperatures and enhances the PCM melting process during the heat input portion of the charge/discharge cycle. Natural convection effects are small during the TES discharge period of the cycle.

7. Receiver and canister performance will be better during ground tests than during on-orbit micro-gravity operation. Therefore, ground test configurations which permit canister heat input "from the side" are suggested to minimize ground versus flight receiver/canister performance differences.

8. An improved two-dimensional PCM canister model along with canister test data is required to quantify the impacts of the void and natural convection on canister thermal performance.

REFERENCES

1. Wilson, D.G.; and Flanery, R.E.: Modeling Cyclic Melting and Refreezing in a Hollow Metal Canister. ORNL-6497, NASA CR-184630, Sept. 1988.

2. Solomon, A.D., et al.: The Development of a Simulation Code for a Latent Heat Thermal Energy Storage System in a Space Station. ORNL-6213, Apr. 1986.

3. Wichner, R.P., et al.: Thermal Analysis of Heat Storage Canisters for a Solar Dynamic, Space Power System. ORNL/TM-10665, Apr. 1988.

4. Solomon, A. D. and Wilson, D. G., "A Stefan-Type Problem With Void Formation and Its Explicit Solution," ORNL-6277, June 1986.

5. Flemings, Merton C., Solidification Processing, McGraw-Hill, 1974.

6. Grodzka, P. G. and Fan, C., "Thermal Control by Freezing and Melting," NASA-CR-120641, March 1968.

7. Borucka, A.: Survey and Selection of Inorganic Salts for Application to Thermal Energy Storage. ERDA-59, U.S. Energy Research and Development Administration, June 1975.

8. Humphries, William R., "Performance of Finned Thermal Capacitors," NASA-TN-D-7690, July 1974.

9. Özisik, M. Necati, Heat Transfer: A Basic Approach, McGraw-Hill, 1985, p. 452-455.

10. Solomon, Alan, "A Note on the Stefan Number in Slab Melting and Solidification," Letters in Heat and Mass Transfer, Vol. 8, 1981, pp. 229-235.

11. Solomon, A. D., "Mathematical Modeling of Phase Change Processes for Latent Heat Thermal Energy Storage," ORNL/CSD-39, August 1979.

12. Strumpf, H.J.; and Coombs, M.G.: Solar Receiver for the Space Station Brayton Engine. J. Eng. Gas Turbines Power, vol. 110, no. 2, Apr. 1988, pp. 295-300.

13. Taylor, M.F.; Bauer, K.E.; and McEligot, D.M.: Internal Forced Convection to Low-Prandtl-Number Gas Mixtures. Int. J. Heat Mass Trans., vol. 31, no. 1, Jan. 1988, pp. 13-25.

14. Thibault, Jules, "Comparison of Nine Three-Dimensional Numerical Methods for the Solution of the Heat Diffusion Equation," Numerical Heat Transfer, Vol. 8, 1985, pp. 281-298.

15. Strumpf, Hal J., and Coombs, Murray G., "Solar Receiver Experiment for the Hybrid Space Station Brayton Engine," ASME Solar Energy Division Conference, San Diego, California, April 1989.

16. Tong, M. T., Kerslake, T. W. and Thompson, R. L., "Structural Assessment of a Space Station Solar Dynamic Heat Receiver Thermal Energy Storage Canister," AIAA SDM Issues of the International Space Station, Williamsburg Virginia, April 21-22, 1988, pp. 162-172.

NASA
National Aeronautics and
Space Administration

Report Documentation Page

1. Report No.
NASA TM-102457

2. Government Accession No.

3. Recipient's Catalog No.

4. Title and Subtitle
Analysis of Thermal Energy Storage Material with Change-of-Phase Volumetric Effects

5. Report Date
January 1990

6. Performing Organization Code

7. Author(s)
Thomas W. Kerslake and Mounir Ibrahim

8. Performing Organization Report No.
E-5244

10. Work Unit No.
474-10-52

9. Performing Organization Name and Address
National Aeronautics and Space Administration
Lewis Research Center
Cleveland, Ohio 44135-3191

11. Contract or Grant No.

13. Type of Report and Period Covered
Technical Memorandum

12. Sponsoring Agency Name and Address
National Aeronautics and Space Administration
Washington, D.C. 20546-0001

14. Sponsoring Agency Code

15. Supplementary Notes

Portions of this material were presented at the 1990 International Solar Energy Conference sponsored by the American Society of Mechanical Engineers, Miami, Florida, April 1-4, 1990. Thomas W. Kerslake, NASA Lewis Research Center; Mounir B. Ibrahim, Dept. of Mechanical Engineering Cleveland State University, Cleveland, Ohio 44115.

16. Abstract

NASA's Space Station Freedom proposed hybrid power system includes photovoltaic arrays with nickel hydrogen batteries for energy storage and solar dynamic collectors driving Brayton heat engines with change-of-phase Thermal Energy Storage (TES) devices. A TES device is comprised of multiple metallic, annular canisters which contain a eutectic composition LiF-CaF_2 Phase Change Material (PCM) that melts at 1040 K. A moderately sophisticated LiF-CaF_2 PCM computer model is being developed in three stages considering one-, two-, and three-dimensional canister geometries, respectively. One-dimensional model results indicate that the void has a marked effect on the phase change process due to PCM displacement and dynamic void heat transfer resistance. Equally influential are the effects of different boundary conditions and liquid PCM natural convection. For the second stage, successful numerical techniques used in the one-dimensional phase change model are extended to a two-dimensional (r,z) PCM containment canister model. A prototypical PCM containment canister is analyzed and the results are discussed. Extension of numerical techniques to a three-dimensional geometry will be reported in the future.

17. Key Words (Suggested by Author(s))
Thermal energy storage; Phase change material;
Enthalpy method; Stefan problem; Void;
Solar dynamic power

18. Distribution Statement
Unclassified – Unlimited
Subject Category 34

19. Security Classif. (of this report)	20. Security Classif. (of this page)	21. No. of pages	22. Price*
Unclassified	Unclassified	33	A03

NASA FORM 1626 OCT 86

*For sale by the National Technical Information Service, Springfield, Virginia 22161

National Aeronautics and
Space Administration

Lewis Research Center
Cleveland, Ohio 44135

Official Business
Penalty for Private Use $300

FOURTH CLASS MAIL

ADDRESS CORRECTION REQUESTED

U.S.MAIL

Postage and Fees Paid
National Aeronautics and
Space Administration
NASA 451

NASA